Proton Switch Correlated with the Morphological Development of the Hydrogen-Bond Network in $H^+(MeOH)_m(H_2O)_1$ ($m = 1-9$): A Theoretical and Infrared Spectroscopic Study

Dan Bing and Jer-Lai Kuo*

School of Physical and Mathematical Sciences, Nanyang Technological University, Singapore 637371, Singapore

Ken-ichiro Suhara, Asuka Fujii,* and Naohiko Mikami

Department of Chemistry, Graduate School of Science, Tohoku University, Sendai 980-8578, Japan

Received: January 4, 2009

A surprising switch of the protonated site from methanol to water in protonated methanol−water mixed clusters, $H^+(MeOH)_m(H_2O)_1$ ($m = 1-9$), was investigated by a joint theoretical and vibrational spectroscopic study. Extensive density functional calculations on all possible structural isomers revealed that the switch of the ion core is correlated with the size dependence and structural development of the hydrogen-bond network: (1) the $CH_3OH_2^+$ ion core is preferred for the small-sized clusters of $m = 1$ and 2, (2) coexistence of the H_3O^+ and $CH_3OH_2^+$ ion cores is highly plausible for $3 \leq m \leq 7$ clusters, and (3) obvious preference of the H_3O^+ ion core appears from $m \geq 8$ with the appearance of the characteristic "tricyclic" structure of the hydrogen-bond network. The ion core switch at $m \approx 8$ is experimentally supported by the infrared photodissociation spectra of the size-selected clusters and the size dependence of the fragmentation channel following vibrational excitation.

Introduction

Since the proposal of the proton-transfer (hopping) mechanism by Grotthuss,[1] microsolvation structures of a proton have attracted much interest with respect to the mobility of the proton in the protic solvents.[2−9] For multicomponents systems, such as methanol−water mixture, the preference of the protonated site has been the subject of extensive studies.[10−27] Though the proton affinity (PA) in the gas phase is a useful index to infer the preferential protonated site, recent gas-phase cluster studies, which provide us clear microscopic structures of the proton solvation, have shown that proton migration can occur from the larger PA site to the smaller PA site with the development of stepwise solvation. This is reasonably explained by the fact that the greater advantage in the solvation compensates for the lower affinity at the bare molecule. For example, Chang and co-workers demonstrated that in $H^+[(CH_3)_2O]_1(H_2O)_n$ the preferential protonated site switches from $(CH_3)_2O$ to water at $n = 2$ in spite of the larger PA of $(CH_3)_2O$ (189 kcal/mol) than that of water (165 kcal/mol).[26] This switch of the protonated site (so-called "proton switch") was attributed to the asymmetric solvation structure of the $(CH_3)_2O$ site. Such results strongly suggest that the proton location in a multiple-component system cannot be determined by a simple push−pull relation between the two molecules neighboring the proton. The preferential location of the proton should be understood in terms of the structural development of the whole hydrogen-bond network.

Protonated methanol−water mixed clusters, $H^+(MeOH)_m(H_2O)_n$ (hereafter abbreviated to $H^+M_mW_n$), are very attractive systems to elucidate the correlation between the preferential proton location and the hydrogen-bond network structure. The PA of methanol (180 kcal/mol) is larger than that of water, but the difference between the magnitudes is much smaller than the cases between water and ketones or amines; therefore, the proton location is expected to be more sensitive to the hydrogen-bond network structure.[28] It has been shown that protonated water clusters (H^+W_n) and protonated methanol clusters (H^+M_m) have very different types of hydrogen-bond network structures ("morphologies"), reflecting the different coordination nature of water and methanol.[29−45] While complicated three-dimensional cage structures are finally favored in H^+W_n, much simpler "bicyclic" structures are the terminal of the "morphological" development in H^+M_m. Mixing of these two components would result in different hydrogen-bond network structures depending on the relative concentration between the two components.

The proton location in $H^+M_mW_n$ has been mainly studied in the two extreme cases, $m \ll n$ (water-rich clusters) and $m \gg n$ (methanol-rich clusters), except the small-sized clusters ($m + n = 4$).[17−19,22−24] Chang and co-workers carried out the pioneering infrared (IR) spectroscopic and theoretical studies of the water-rich clusters ($m = 1$, $n = 1-6$) as well as the small-sized $m + n = 4$ clusters to elucidate their detailed hydrogen-bond structures.[17,24] They identified the existence of the $CH_3OH_2^+$ (abbreviated to $MeOH_2^+$), H_3O^+, and $CH_3OH-H^+-(H_2O)_2$ ion cores. The preferential protonated site sensitively depends on the cluster size and hydrogen-bond structure. Coexistence of the $MeOH_2^+$ and H_3O^+ ion cores was observed in the small-sized clusters ($m + n \leq 4$) at the finite temperature. We also recently reported the correlation between the proton location and hydrogen-bond network morphology in the water-rich clusters of the relatively larger sizes ($m = 1$, $n = 1-9$, and 21).[20,46] Because of the difference of the preferential coordination numbers of the ion cores (2 for $MeOH_2^+$ but 3 for H_3O^+), the development of the hydrogen-bond network into the 3-D cage structures in the water-rich clusters induces the exclusive location of the proton on the water site.

* To whom correspondence should be addressed. E-mail: JLKuo@ntu.edu.sg (J.-L.K.); asukafujii@mail.tains.tohoku.ac.jp (A.F.).

10.1021/jp900066u CCC: $40.75
Published on Web 02/24/2009

In contrast to the extensive spectroscopic and theoretical studies in the water-rich clusters, the proton location in the methanol-rich clusters has been mainly discussed only on the basis of mass spectrometric and thermochemical studies.[14−16,21−23,47] Kebarle et al. first carried out the mass spectrometric study of $H^+M_mW_n$.[14] On the basis of the cluster size distribution, the preferential solvation of the proton by water was predicted for the larger-sized clusters, while coexistence of both ion cores was suggested for the smaller-sized clusters ($m + n \leq 6$). Stace and co-workers measured the metastable decay of $H^+M_mW_1$ and found the switch of the preferential fragmentation channel with the cluster size. While in the $m < 9$ clusters water loss is the dominant fragmentation channel, the methanol loss becomes dominant at $m \geq 10$.[15,16] These results were interpreted as the proton switch occuring from the $MeOH_2^+$ ion core to the H_3O^+ ion core at $m \approx 9$ because of the lower evaporation possibility for the protonated site. On the other hand, Meot-Ner measured the enthalpy change in the stepwise replacement of water by methanol. In every step from H^+W_7 to H^+M_7, the replacement was exoenergetic, and preferential solvation of the proton by methanol was concluded up to $m = 7$.[21] Garvey and co-workers observed the magic number behavior of $H^+M_mW_1$ and $H^+M_mW_2$ at $m = 9$ and 10, respectively, and proposed the formation of a characteristic "inclusion" structure at the magic number, where the H_3O^+ (or $H_5O_2^+$) ion core is surrounded by a methanol ring. They also measured the collision-induced dissociation of $H^+M_mW_1$ and reported the change of the preferential dissociation channel from the water loss at $m \leq 8$ to the methanol loss at $m \geq 9$.[23] This was interpreted as evidence for the proton switch from $MeOH_2^+$ to H_3O^+. Jackson recently reported the mass distribution of the larger-sized $H^+M_mW_n$ mixed clusters and supported the suggestion by Garvey et al.[47]

All these mass spectrometric studies strongly suggested the characteristic ion core switching at $m \approx 9$. However, proton migration prior to dissociation can obscure the actual critical size of the switching. Moreover, detailed structural information on the hydrogen-bond network is hardly extracted from the mass spectrometric results. Systematic consideration of the proton switch along with the hydrogen-bond network morphology development has never been given except the qualitative assumption of the characteristic inclusion structure formation to explain the critical size for the proton switch.[22,23] Collaboration between theoretical calculations and infrared spectroscopy is expected to give us unequivocal structural information also for the methanol-rich clusters. However, IR spectroscopic studies on methanol-rich mixed clusters have been limited to small-sized clusters, $H^+M_4W_1$ and $H^+M_3W_1$, by Chang and co-workers.[18,24] Recently, we carried out IR spectroscopy and extensive theoretical calculations of H^+M_m and established the fundamental process of the morphological development of the hydrogen-bond network of H^+M_m.[30,31] We demonstrated that structures of H^+M_m are much simpler in comparison with those of H^+W_n because of the lower flexibility in the coordination of methanol. Mixing of a single water molecule to H^+M_m allows more flexibility in the hydrogen-bond network structure construction as well as the proton location.

In the present study, on the basis of the previous analysis of H^+M_m, we explore the proton switch correlated with the morphological development in $H^+M_mW_1$ by both density functional theory (DFT) calculations and IR spectroscopic measurements. Energy-optimized structures of $H^+M_mW_1$ ($m = 1-9$) are extensively searched in the systematic manner, and their relative energies and zero-point vibrational energy corrections are evaluated. Coexistence of structural isomers is discussed on the basis of the Gibbs free energy evaluation. IR spectra of the clusters are experimentally measured for $m = 3-9$ in the 3 μm region. IR spectral simulations are also carried out, and they are compared with the observed spectra. Dissociation fragment channels following vibrational excitation are also discussed in terms of the preferential proton location.

Computational Methods

Geometries of $H^+(MeOH)_m(H_2O)_n$ were optimized at the B3LYP/6-31+G* level using the Gaussian 03 program package.[48] The reliability of this level of calculations for protonated clusters has been well established by previous studies.[2,31,35] For each energy-optimized structure, the frequency calculation was performed to confirm the geometry is an energy minimum, and the zero-point energy (ZPE) correction was estimated by the harmonic approximation ($ZPE \cong \sum_i \hbar\omega_i/2$). To access the thermal effects, we also calculated the Gibbs free energy at 190 K, which is the estimated temperature of the protonated clusters in the present experimental measurements.

As for the initial input structures for the energy optimization, we employed two methods. For the small-sized clusters of $m \leq 3$, several structures can be formed. These structures can be constructed manually. However, both the complexity in structures and the number of acceptable conformations within a given structure significantly increase with the cluster size. In the construction of a wide variety of input structures for large-sized $H^+M_mW_1$, we rely on our previous experience with H^+W_n and H^+M_m.[31,32] An input structure of an isomer of $H^+M_mW_1$ can be easily obtained by replacing a methanol by a water from H^+M_{m+1} or replacing m water molecules (except for the water sites of which coordination is unreasonable for methanol) by methanol from H^+W_{m+1}.

Experimental Methods

IR spectra of $H^+M_mW_1$ ($m = 3-9$) were experimentally recorded by IR predissociation spectroscopy using a mass spectrometer which was equipped with linearly aligned tandem quadrupole mass filters connected by an octopole ion guide. The details of the apparatus have already been described in the previous papers,[30,31] and only a brief description is given here. $H^+M_mW_1$ was produced by a photoassisted discharge of the methanol/water mixed vapor seeded in the Ne buffer gas (total pressure of 3 atm). The gaseous mixture was expanded from a pulsed supersonic valve through a channel nozzle. The channel was equipped with a pin electrode at its sidewall, and a direct current voltage of −300 V relative to the channel was applied to the electrode. The discharge in the channel was triggered by irradiation of the electrode surface with a laser pulse (355 nm, 5 mJ/pulse), which is synchronized with the pulsed valve operation. The $H^+M_mW_1$ cluster cations were cooled through the expansion from the channel. The cluster cations were size selected by the first quadrupole mass filter, and then they were introduced into the octopole ion guide. The mass resolution of the first mass filter was set to be higher than 1 amu to exclude contamination of undesired cluster species. Within the octopole ion guide, the mass-selected cluster cations were irradiated by a counter propagating IR laser and sent to the second quadrupole mass filter, which was tuned to pass only the mass of the H^+M_m (water loss) or $H^+M_{m-1}W_1$ (methanol loss) fragment ion produced by vibrational excitation. Thus, an IR spectrum of the size-selected cluster was recorded by monitoring the fragment ion intensity while scanning the IR laser frequency. The IR light was generated by difference frequency mixing (DFM) between the fundamental outputs of a YAG laser and a dye laser.

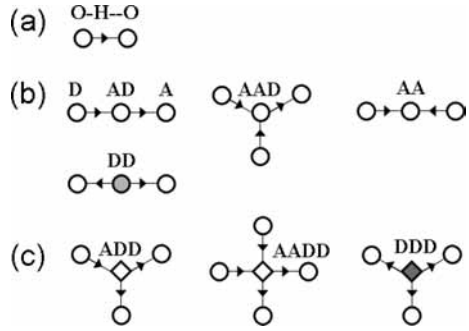

Figure 1. Definitions of the symbolic representation of hydrogen bonds and building block patterns of the hydrogen-bond coordination (see text). (a) Definitions of the symbolic representation. The oxygen atom in methanol is represented by an open circle, and the methyl group and hydrogen atoms are omitted in the representation. An arrow indicates a hydrogen bond that binds two oxygen atoms. The direction of the arrow shows the donor−acceptor relation in the hydrogen bond. (b) Possible coordination types for methanol and protonated methanol sites. The oxygen atom of the protonated site is represented by a closed circle. (c) Characteristic coordination types for water and protonated water sites. The oxygen atoms of the water and protonated water sites are represented by open and closed diamonds, respectively.

Results and Discussions

A. Symbolic Hydrogen-Bond Representations and Coordination Types of the Building Blocks. In our previous study on H^+M_m, we introduced a simple symbolic representation for a hydrogen bond, which is helpful to consider structural development of a hydrogen-bond network.[30,31] Figure 1a shows its definitions. A hydrogen bond is represented by an arrow between proton-donating and -accepting oxygen atoms. Oxygen atoms of methanol molecules are represented by open circles, and all the hydrogen atoms and methyl groups are omitted. The donor−acceptor relation of the hydrogen bond is represented by the direction of the arrow (from a proton donor to a proton acceptor). The oxygen atom of the water molecule is represented by an open diamond. A closed circle or closed diamond represents the oxygen atom in the ion core site. By using these definitions, the possible coordination types of methanol and water are summarized as shown in Figure 1b and 1c. A methanol molecule can be a proton acceptor (A), proton donor (D), double acceptor (AA), single acceptor single donor (AD), or double acceptor single donor (AAD) site. For water, on top of all the possible coordination types in methanol, double donor (DD), single acceptor double donor (ADD), and double acceptor double donor (AADD) are acceptable coordination types.

Exceptional coordination types should be also considered only for the ion cores. For example, D, AD, DD, and ADD are acceptable coordination types for $MeOH_2^+$. However, it has been shown in previous studies on H^+W_n, H^+M_m, and $H^+M_1W_n$ that the coordination of the ion cores shows strong preferences.[20,31,32,46] The $MeOH_2^+$ ion core has a strong preference to take up the DD form. This tendency is reasonably understood as follows: the D type means the $MeOH_2^+$ ion core is under coordinated, and it is stable only in very small-sized clusters. On the other hand, AD and ADD are not stable since it requires the positively charged $MeOH_2^+$ ion core to accept a proton from another neutral donor. No stable AD and ADD coordination of $MeOH_2^+$ has been found in $H^+M_1W_n$ and H^+M_m. For the same reason, the H_3O^+ ion core prefers the triple donor (DDD) coordination, and D and DD can be formed only in small-sized clusters before full solvation of the ion core. The AD, ADD, and single acceptor triple donor (ADDD) types have never been found for the H_3O^+ ion core.

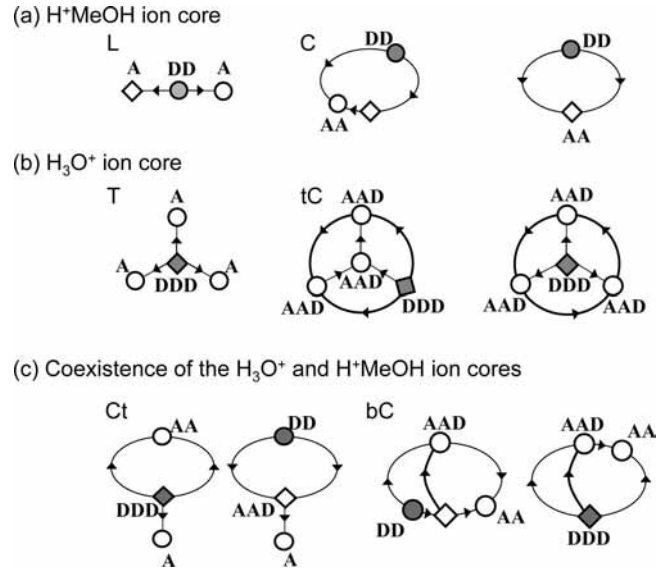

Figure 2. Schematic representations of the six basic morphologies of $H^+(MeOH)_m(H_2O)_1$ ($H^+M_mW_1$). The symbolic representation of the hydrogen bond defined in Figure 1 is employed, and all the AD sites are neglected in the representations for simplicity. (a) Morphologies only with the $MeOH_2^+$ ion core. (b) Morphologies only with the H_3O^+ ion cores. (c) Morphologies having both types of the ion cores.

B. Possible Morphologies. It is reasonably anticipated that the structures of the methanol-rich clusters $H^+M_mW_1$ should be similar to those of H^+M_m. We previously demonstrated the basic morphology development process of H^+M_m, and it is briefly summarized in Figure 2 with the symbolic representation of the hydrogen-bond network.[30,31] The simplest morphology is linear structures (L). Starting with the DD configuration of the ion core, AD sites extend the one-dimensional chains, which are terminated by two A sites. When these two terminal A sites are bound to each other, one site becomes an AD site and the other is transformed to an AA site. Then, the morphology is developed from L to cyclic structures (C). A hydrogen-bond chain can be extended from the AA site (the AA site is then transformed to the AAD site), and such structures are categorized into cyclic structures with a "tail" (Ct). This chain has special importance in structure development because it is terminated with an A site and can be bound to an AD site in the ring moiety (even if there are other side chains in the ring moiety, they are terminated only with D sites and cannot be bound anywhere in the hydrogen-bonded network). When the "tail" in the Ct structures is bound to the ring moiety, the ring is bridged and the morphology is developed to bicyclic structures (bC), which are the terminal of the morphological development in H^+M_m.

Addition of a single water molecule into H^+M_m enriches the structure types because of the diversity of the coordination types of water. Not only the L, C, Ct, and bC structures in H^+M_m but also two more new types can be formed in $H^+M_mW_1$. One is tree structures (T), which are favored for the H_3O^+ ion core due to its full solvation. The double (triple) proton-donating ability of the water (protonated water) site enables producing one more side chain ('tail') which is terminated by an A site, in comparison with the cases of H^+M_m. Therefore, two bridges across the ring moiety can finally occur in $H^+M_mW_1$. Then, the cyclic moiety is segmented into three parts in such structures, and we categorize this structural type to tricyclic structures (tC). The inclusion structures proposed by Garvey and co-workers are involved in this category.[22,23] Existence of a single water

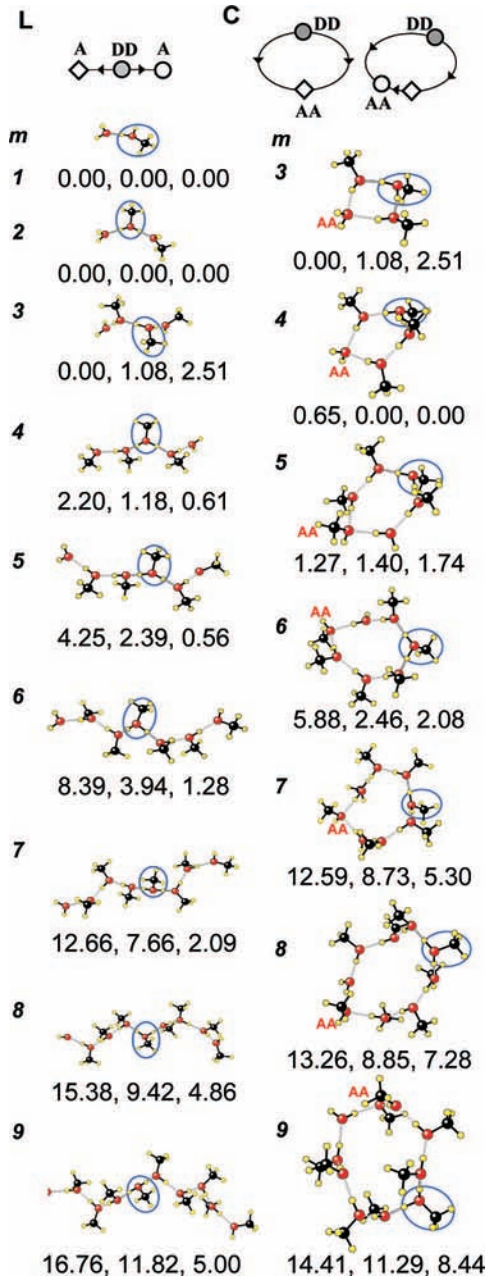

Figure 3. Most stable structures of morphologies with the methanol ion core, "linear" (L) and "cyclic" (C) (left and right columns, respectively). The values below the structures are the relative E_0 (the first number), the relative E_0 + ZPE (the second number), and the relative Gibbs free energy at 190 K (the third number) computed at B3LYP/6-31+G* (in kcal/mol). The zero of these energy scales is set to the energy of the most stable isomer in each size. The positions of the methanol ion core are highlighted with the blue circles. The complete list of isomers is given in the Supporting Information.

molecule also enables several different hydrogen-bond network patterns in the Ct and bC structures.

C. Stable Isomers of $H^+M_mW_1$. In this study, we systematically searched stable isomer structures of $H^+M_mW_1$ for m = 1−9. In Figures 3−5, we summarize the most stable isomer of each size and morphology. The complete list of obtained stable structures is seen in the Supporting Information.

Because of the strong preference for the full solvation of the ion core moiety, all of the most stable isomers of the L and C structures have the $MeOH_2^+$ ion core while those of the T and tC structures have the H_3O^+ ion core. In the Ct and bC structures, both ion cores are found in the most stable isomers, depending on the cluster size. In the following, we overview the trends of the most stable isomer structure in each cluster morphology.

1. Morphologies with the $MeOH_2^+$ Ion Core.

Linear Structures (L). Similar to the H^+M_m and H^+W_n clusters, L structures are the simplest and most basic form of $H^+M_mW_1$. The excess proton is found to prefer to reside at the central methanol site of the hydrogen-bond network to stabilize the strong hydrogen bonds around the ion core. In the L structures, the H_3O^+ ion core is not favored because of the lack of full solvation. The water molecule is found to prefer staying at the terminal of the linear structure for all sizes.

Cyclic Structures (C). Cyclic structures are energetically more favorable only in the small sizes up to 6. The excess proton prefers residing on the methanol site due to the similar reason in the L structures. Both the AA site and water molecule favor to be away from the ion core. This trend has also been found in H^+M_m.[31]

2. Morphologies with the H_3O^+ Ion Core.

Tree Structures (T). T structures are characteristic to the H_3O^+ ion core because the DDD coordination (full solvation) of the H_3O^+ ion core is satisfied in these structures. The methanol molecules favor even distribution of the three branch lengths. The T structure with a $MeOH_2^+$ ion core and an AAD methanol branching site is not stable, which is indicated in previous work that there is no T structure in H^+M_m.[31] The T structures with an AAD water branching site is also not stable, and that with an ADD water branching site are higher in energy. The same trends were seen in $H^+M_1W_n$.[46]

Tricyclic Structures (tC). These particular structures maximize the number of hydrogen bonds (no free (dangling) OH exists) in clusters with full solvation of the H_3O^+ ion core. Though it is also geometrically possible to construct tC structures with the $MeOH_2^+$ ion core, only the H_3O^+ ion core was found in the stable isomers. Depending on the location of the ion core, there are two types of structures, as schematically shown in Figure 2. One has the ion core at the center of the hydrogen-bond network (the "inclusion" structure). In the other type, the ion core locates on the "outskirt" (the largest ring) of the hydrogen-bond network. To explain the magic number behavior of $H^+M_9W_1$, Garvey and co-workers suggested the former type of the tC structure.[22,23] In the present calculations, the tC structure is found to exist from m = 6, because 6 is the minimum number to include another molecule in the hydrogen-bonded ring. Moreover, we found that the latter ("outskirt") type of tC isomer is more stable than the former ("inclusion") type in each size, as shown in Figure 4. In the 3-D cage structures of H^+W_n, it has been suggested that the excess proton prefers locating on the surface site rather than the interior site.[20,32,35,37−39] The similar trend was observed for the tC structures.

Although the tC structures are not flat, their network topology is essentially two-dimensional. For m = 6, the structure is more symmetric with one methanol in the center and the six other molecules in the outer ring. The big ring is segmented into three 4-membered rings. For larger sizes, the structures can be constructed by adding AD methanols to $H^+M_6W_1$. In Figure 4a, two kinds are constructed for the more stable "outskirt" type according to the location of added AD molecules. For (a)-1, AD molecules are added to the inner segments, while for (a)-2, AD molecules are added to the outer ring. The calculated relative energies show that (a)-1 is more stable with the fact that more molecules are put near the ion core. Our results show that this "outskirt" tC with the 6-membered outer ring is the most stable structure for m = 6−9.

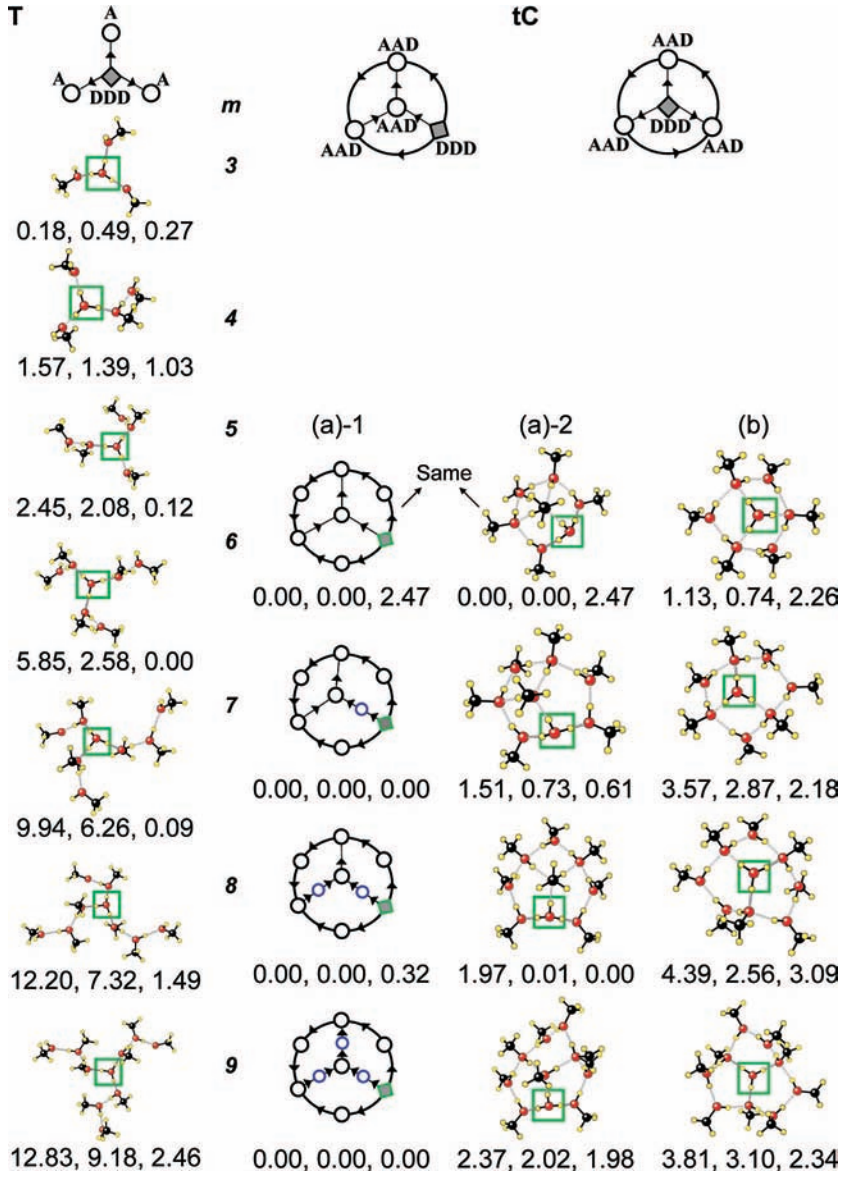

Figure 4. Energy-optimized stable structures of morphologies with the water ion core, "tree" (T) and "tricyclic" (tC). Two types are presented for tC structures in the figure. (a) With the H_3O^+ ion core in the outskirt (largest) hydrogen-bond ring. ((a)-1) For $m \geq 7$, the structures are constructed by adding methanol molecules (blue one) to the inner segments of $H^+M_6W_1$. Schematic structure representations are used to present clearly. (Different from Figure 2, all the molecules are presented including the AD molecules.) ((a)-2) Constructed by adding methanol molecules to the outskirt of $H^+M_6W_1$. (b) With the H_3O^+ ion core in the center. Note the latter is less stable than the former (see text). The values below the structures are the relative E_0 (the first number), the relative E_0 + ZPE (the second number), and the relative Gibbs free energy at 190 K (the third number) computed at B3LYP/6-31+G* (in kcal/mol). The positions of the water ion core are highlighted with the green squares. The complete list of isomers is given in the Supporting Information.

3. Morphologies with the Coexistence of the $MeOH_2^+$ and H_3O^+ Ion Cores.

Cyclic with a Tail (Ct). Two different hydrogen-bond network patterns are found in the stable isomers of this structural category. As shown in Figure 2, one has the $MeOH_2^+$ ion core separated far from the 3-coordinated ADD water, which is the branching site to have the "tail". The other type has the 3-coordinated DDD H_3O^+ ion core with the AA methanol site far from the ion core. The "tail" arises from the ion core. The most stable structures depend on the cluster size as shown in Figure 5, and there is no clear trend on the preference of the ion core.

Bicyclic (bC). Unlike the above types of structures, bicyclic structures are complicated and have higher energy, as shown in Figure 5. Only two types are presented. Both the water and the methanol ion cores coexist.

D. Relative Stability. The electronic potential energy (E_0), total energies (E_0 + ZPE), and Gibbs free energy (G) at 190 K are evaluated for all stable structures. The energy evaluation was carried out at the B3LYP/6-31+G* level with the standard harmonic approximation. For E_0, E_0 + ZPE, and G, those of the minimum energy isomer in each cluster size (m) are set to zero. The relative values among the different structures are shown in Figures 3−5 and also summarized in Figure 6.

The E_0 values in Figure 6a are scattered with the increase of the size, and they finally span a range of ~17 kcal/mol at m = 9. As the cluster size increases, more "compact" structures (bC and tC) tend to gain greater binding energy. This is especially clear for the tC structure, having more than 8 kcal/mol lower energy than the next stable one at m = 8 and 9. This trend is in line with the fact that there are more

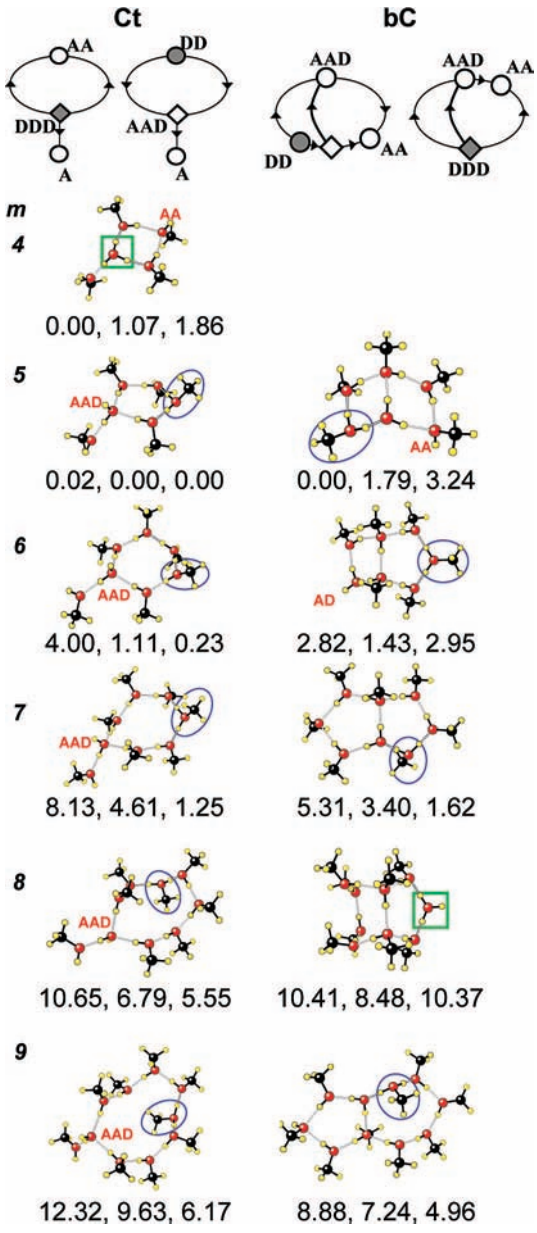

Figure 5. Most stable structures of morphologies with both the methanol and the water ion cores, "cyclic with a tail" (Ct) and "bicyclic" (bC) (left and right columns, respectively). The values below the structures are the relative E_0 (the first number), the relative E_0 + ZPE (the second number), and the relative Gibbs free energy at 190 K (the third number) computed at B3LYP/6-31+G* (in kcal/mol). The complete list of isomers is given in the Supporting Information.

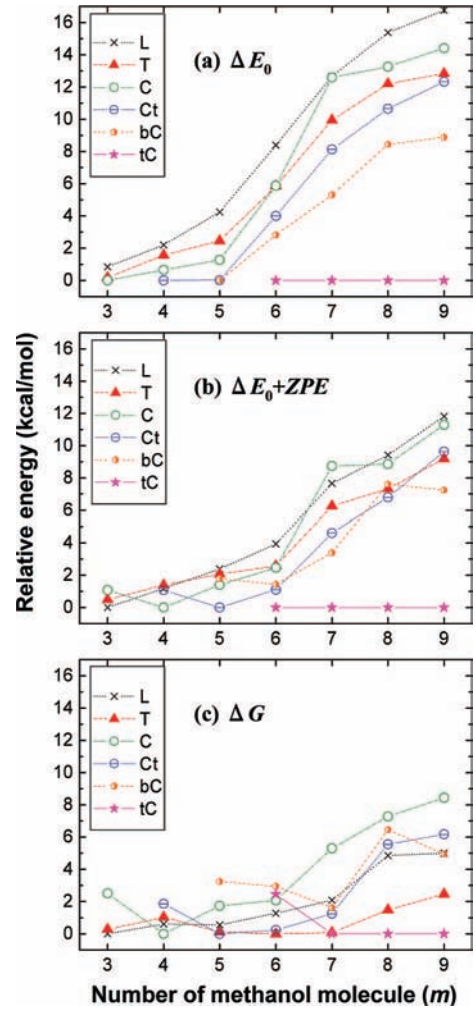

Figure 6. Relative stabilities (in kcal/mol) of the most stable isomers of each morphology of $H^+M_mW_1$ ($m = 3-9$). The cluster size (m) is indicated by the x axis. (a) Relative potential energies (E_0). (b) Relative energies at the zero vibrational level (E_0 + ZPE). (c) Relative Gibbs free energies at 190 K.

hydrogen bonds in the compact structures in comparison with the "open" structures (L, T, C, and Ct).

The relative stability of the clusters at 0 K is determined by the competition between ΔE_0 and ΔZPE. The compact structures tend to have larger ΔZPE values because of their higher vibrational frequencies due to the relatively rigid structures, while flexibility of the open structures results in the relatively lower vibrational frequencies. The same trend has been found for H^+W_n, H^+M_m, and water-rich $H^+M_mW_n$ clusters.[31,32,46] The energy difference at the zero-point level (ΔE_0 + ΔZPE) is shown in Figure 6b, and its magnitude becomes smaller (~12 kcal/mol) than ΔE_0 due to the opposite trends between ΔE_0 and ΔZPE. At 0 K, the energy difference is estimated to be very small in the small-sized clusters ($m \leq 5$), but the large advantage of the tC structure is still seen at $m \geq 7$.

To access the thermal effects on the relative stability, the Gibbs free energies at 190 K are also calculated. The temperature of 190 K is the estimated temperature of the protonated clusters in the present experimental measurements. The calculated Gibbs free energy in Figure 6c favors the open structures (L, T, C, and Ct) at small sizes ($m \leq 7$), because of rich low-frequency modes. On the other hand, the tC and T structures have much lower Gibbs free energies than the others at $m \geq 8$. The differences among the Gibbs free energies of the different structures are ~ 8 kcal/mol at 190 K.

As seen from the small Gibbs energy differences, the coexistence of multiple isomers is highly plausible for the small-sized clusters ($m \leq 7$). For $m = 1$ and 2, $H^+M_mW_1$ has only linear structures, and the $MeOH_2^+$ ion core is preferred. For $m = 3-7$, the $MeOH_2^+$ and H_3O^+ ion cores would coexist because of the small energy difference among the multiple isomers. However, the tC and T structures have much lower Gibbs free energy (~3 kcal/mol) than the others for $m \geq 8$. Because both of these structures only have the H_3O^+ ion core, the preference of the H_3O^+ ion core for the clusters of $m \geq 8$ is clearly seen. The previous mass spectrometric studies of $H^+M_mW_1$ suggested that the proton switch occurs from the $MeOH_2^+$ ion core to the H_3O^+ ion core at $m \approx 9$.[14,22] The present theoretical calculations support this suggestion well. The small difference of the critical

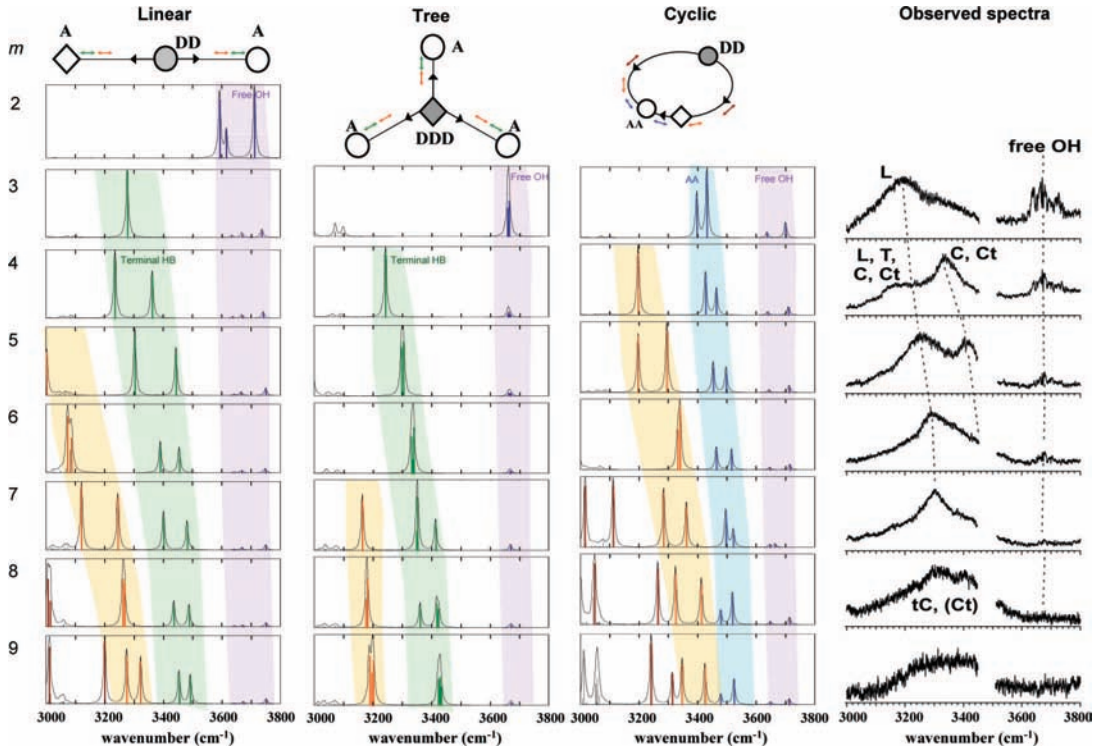

Figure 7. Simulated infrared vibrational spectra on the basis of the most stable optimized structures of L, T, and C morphologies (left) and observed infrared spectra (right) of $H^+M_mW_1$. All calculations were carried out at B3LYP/6-31+G* (rescaled by the scaling factor of 0.973). The vibrational bands are color coded with the vibrational modes shown in the schematic representation of the morphologies, and the stripes are made for eye-guiding purposes. In the observed spectra, the water loss channel was monitored for the spectra of $m = 3-8$, while the methanol loss channel was monitored for the spectra of $m = 9$ (see text).

size of the switching exists between the observation ($m \approx 9$) and theoretical prediction ($m \approx 8$). It would come from the temperature of the observed clusters as well as the precision of the energy evaluation in the DFT level calculations. The tC structures are predicted to be the terminal of the morphological development, which is consistent with previous studies. However, it should be noted that the most stable isomers in large clusters are of the "outskirt" structures and not of the "inclusion" structures assumed in the previous studies.[22,23] In summary, the present calculations clearly demonstrate the trend of the proton switch in $H^+M_mW_1$ correlated with morphological development.

E. DFT Simulations of Vibrational Spectra and Comparison with Observed Vibrational Spectra. Figures 7 and 8 show the simulated and observed IR spectra of $H^+M_mW_1$ in the 3 μm region. The observed spectra are shown in the rightmost column in each figure. The same observed spectra are reproduced in both Figures 7 and 8 for convenience of comparison with the simulations. The simulations are on the basis of the most stable isomer of each structure. All calculated harmonic frequencies are scaled by a factor of 0.973, which is determined to reproduce the free OH-stretch band in neat and protonated water clusters.[49] The stick spectra are converted into the continuous spectra by convolution with a Lorentzian function of 10 cm^{-1} full width at half-maximum. On the other hand, the observed spectra were measured by using the dissociation spectroscopic technique, and the water loss channel (H^+M_m fragment) and methanol loss channel ($H^+M_{m-1}W_1$ fragment) were monitored for spectra of $m = 3-8$ and $m = 9$, respectively. As will be discussed in the next subsection, no clear difference of the spectral feature was found by monitoring the different dissociation channels. The gaps in the observed spectra at the 3440−3520 cm^{-1} region are due to the IR absorption of the nonlinear optical crystal, which is used to generate the IR light.

First, we overview spectral features in the simulations. In the frequency range of 3000−3600 cm^{-1}, strong bands due to hydrogen-bonded OH stretches are expected. Two different size-dependent trends are seen in these bands. As seen in Figures 7 and 8, the hydrogen-bonded OH stretch bands in the L, T, C, and Ct structures show a clear tendency to be blue shifted as the cluster size increases. The blue shifts demonstrate the reduction of the hydrogen-bond strength, and their origin is attributed to the increase of the average distance from the ion core and associated charge delocalization.[46] On the other hand, as shown in Figure 8, the slight red shifts with an increase of the size are seen in the tC structure. In such compact structures, the distortion of the hydrogen-bond angle in the ring moieties is reduced with the increase of the size. These red shifts indicate the enhancement of the hydrogen-bond strength with the reduction of the distortion. The similar effects on the hydrogen-bonded OH stretches have been found in the IR spectra of H^+M_m.[31] Above 3600 cm^{-1}, the free OH stretch bands are expected in all the structures except the tC structure. The absence of the free OH stretch band in the tC structure reflects that all the OH groups are hydrogen bonded in this structure, and this is a unique spectral sign of the tC structure.

In the observed spectra, significant band broadening occurs in the hydrogen-bonded OH stretch region, but some clear band structures are seen. In $m = 3$, the broad absorption observed around 3200 cm^{-1} is attributed to the hydrogen-bonded OH stretch of the L structure. Though the T structure is also expected to be competitive, no hydrogen-bonded OH band is predicted in this region (the hydrogen-bonded OH stretches of the H_3O^+ ion core locate in the much lower frequency region). In $m = 4$ and 5, two broadened bands are observed in the 3200−3400 cm^{-1} region. Both bands show blue shifts with an increase of the size. As shown in the simulations, such blue shifts are

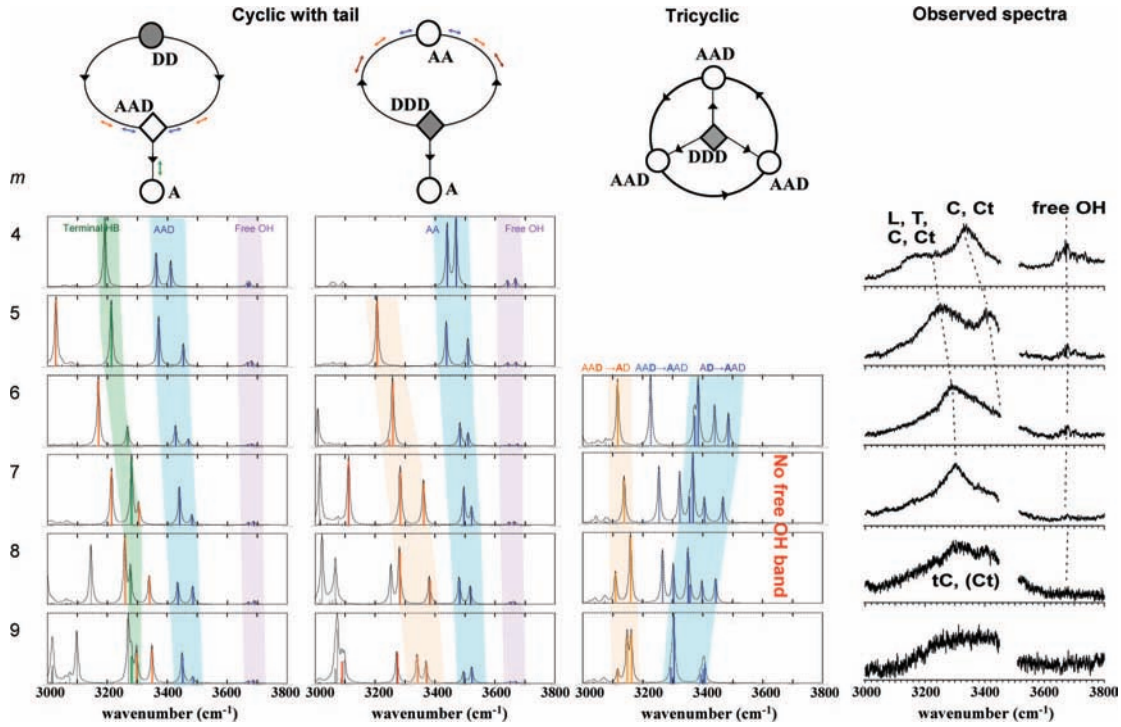

Figure 8. Simulated infrared vibrational spectra on the basis of the most stable optimized structures of Ct and tC morphologies (left) and observed infrared spectra (right) of $H^+M_mW_1$. All calculations were carried out at B3LYP/6-31+G* (rescaled by the scaling factor of 0.973). The vibrational bands are color coded with the vibrational modes shown in the schematic representation of the morphologies, and the stripes are made for eye-guiding purposes. The observed spectra are reproductions of those in Figure 7 for convenience of comparison with the simulations.

characteristic to the "open" structures. The lower frequency band (3200−3300 cm^{-1}) is attributed to the hydrogen-bonded OH stretches of the L, T, C, and Ct structures, and the higher frequency band (3300−3400 cm^{-1}) is to the C and Ct structures, which would become competitive in this size region at 190 K (as seen in Figure 6c). The dominance and coexistence of the "open" isomers in the small size range is strongly suggested by the Gibbs energy evaluation, and the observed spectra are consistent with this expectation. The higher frequency band due to the C and Ct structures almost disappears in $m = 6$. This disappearance may be due to the decrease of the relative intensity of this band as seen in the simulations. The hydrogen-bonded OH stretch features seem to converge to a much broadened band centered at ~3400 cm^{-1} in $m \gtrsim 6$. This is also consistent with the convergence of the blue-shifting hydrogen-bonded OH stretch bands of the "open" isomers into this frequency region. Though the proton switch, i.e., exclusive H_3O^+ ion-core formation, is expected at $m \approx 8$, no drastic change of the spectra is seen in this size region. Isomers of the "compact" structures also show rich band features around the 3400 cm^{-1} region, and it may be the reason for the absence of the clear spectral sign reflecting the proton switch. The broadened band due to the coexistence of the isomers of multiple structures in $m \lesssim 7$ would smoothly change to that attributed to the rich hydrogen-bonded features of the tC structure in $m \gtrsim 8$.

The dominant contribution of the tC structure in $m \gtrsim 8$ is, however, supported by the size dependence of the free OH stretch band observed at around 3670 cm^{-1}. No free OH group exists in the tC structure, and the disappearance of the free OH band is an indication of the dominant contribution of the tC structure. The free OH band intensity in the observed spectra decreases with the increase of the cluster size, and it almost disappears at $m = 7-8$. This observation is consistent with the Gibbs energy evaluation and previous mass spectrometric suggestion.[22,23]

TABLE 1: Relative Branching Ratios of the Dissociation Channels of $H^+M_mW_1$ Following Vibrational Excitation at 3360 cm^{-1}

m	H_2O loss	MeOH loss
4	0.95	0.05
5	0.95	0.05
6	0.90	0.10
7	0.90	0.10
8	0.60	0.40
9	0.30	0.70
10	0.00	1.00

F. Dissociation Channels Due to the Vibrational Excitation. In the previous mass spectrometric studies of $H^+M_mW_1$, the proton switch has been suggested on the basis of the size dependence of the dissociation channels in the metastable clusters or in the collision-induced dissociation.[14−16,22,23] In the present study, we also examined the dissociation channels following vibrational excitation.

In the size range of $m = 4-9$, we measured the IR spectra by monitoring both of the water loss channel (H^+M_m fragment) and the methanol loss channel ($H^+M_{m-1}W_1$ fragment). The comparison of the spectra are seen in the Supporting Information, and no clear spectral difference between the monitoring channels was found in both the free and hydrogen-bonded OH regions, except the free OH stretch bands of $m = 4$. Chang and co-worker already reported this exceptional behavior of $m = 4$.[18] Because the essentially same band feature was observed by monitoring the water loss and methanol loss channels, we fixed the IR laser wavelength to 3360 cm^{-1}, around the maximum absorption in every cluster size and measured the relative branching ratios of the dissociation channels. The observed relative ratios between the two dissociation channels are shown in Table 1. While the water loss is the major dissociation channel in the small-sized clusters of $m \leq 7$, the methanol loss channel becomes predominant in $m \geq 8$. This is

consistent with our calculated Gibbs energy evaluation and the observed vibrational spectra.

Irrespective of the relative branching ratio, no dissociation channel dependence was observed for the IR spectral features. This indicates that the vibrational excitation causes extensive migration of the isomer structure prior to dissociation. The migration would include the proton switch and wash out the correlation between the initial proton location and preferential dissociation channel. Therefore, the branching ratio would be a (partial) reflection of the statistical weight during the dissociation process, and it cannot be simply transformed into the relative population of the proton location before the vibrational excitation. The preferential methanol loss in the larger-sized clusters, however, is consistent with the theoretical prediction of their preference of the H_3O^+ ion core. The small difference of the critical size in comparison with the previous mass spectrometric study ($m = 9$) would be attributed to the difference of the available energy in the dissociation process as well as to the cluster temperature at the ion source.

Conclusions

Extensive DFT calculations of the $H^+M_mW_1$ clusters were carried out. The systematic search of the most stable isomer structure in various morphologies of the clusters clearly demonstrated the correlation between the cluster morphology and the preferential location of the protonated site. The size-dependent development of the hydrogen-bond network of the clusters was examined. The calculation results showed that the L structure and the $CH_3OH_2^+$ ion core is preferred for the small-sized clusters of $m = 1$ and 2. The coexistence of multiple structures and different ion cores ($MeOH_2^+$ and H_3O^+) was suggested for the small-sized clusters of $3 \leq m \leq 7$. Compared with the H^+M_m, adding one water molecule will encourage the formation of two new morphologies, T and tC structures. Both T and tC, which have only the H_3O^+ ion core, were shown to be preferential in $m \geq 8$, consistent with the previous mass spectrometric results. The IR spectra of the clusters were simulated and compared with the observed spectra in the OH stretching vibrational region. The spectral features of the observed spectra were well interpreted by the spectral simulations with the coexistence of the multiple isomers at small sizes. The disappearance of the free OH stretch band shows the dominant contribution of the tC structure (having the H_3O^+ ion core) at $m = 7-8$. The dissociation channel branching ratio due to vibrational excitation also supported the preference of the H_3O^+ ion core for $m \geq 8$. All results from our calculation, observed IR spectra, and dissociation channel measurements suggest that the proton switch from the $MeOH_2^+$ ion core to the H_3O^+ ion core occurs at $m = 8$ in $H^+M_mW_1$. The small difference of the critical size of the switching between the others' work ($m \approx 9$)[14,22] and this work ($m \approx 8$) would come from the temperature of the observed clusters as well as the precision of the energy evaluation in the DFT level calculations.

Acknowledgment. This work was supported in part by Nanyang Technological University and the Ministry of Education of Singapore under URC Grants (RG34/05 and RG57/05), the Grant-in-Aid for Scientific Research (KAKENHI) on Priority Areas "Molecular Science for Supra Functional Systems" [477] from MEXT, Japan, the KAKENHI Project Nos.19056001 and 20550005 from JSPS, Japan, and the Mitsubishi Foundation.

Supporting Information Available: IR spectra obtained by monitoring the water loss and methanol loss channels, complete list of isomers of $H^+(MeOH)_m(H_2O)_1$ ($m = 1-9$) along with their relative energies, and complete ref 48. This material is available free of charge via the Internet at http://pubs.acs.org.

References and Notes

(1) Grotthuss, C. J. T. d. *Ann. Chim. Phys.* **1806**, *58*, 54.
(2) Jiang, J. C.; Wang, Y. S.; Chang, H. C.; Lin, S. H.; Lee, Y. T.; Niedner-Schatteburg, G.; Chang, H. C. *J. Am. Chem. Soc.* **2000**, *122*, 1398.
(3) Stoyanov, E. S.; Stoyanova, F. V.; Reed, C. A. *Chem. Eur. J.* **2008**, *14*, 3596.
(4) Rasaiah, J. C.; Garde, S.; Hummer, G. *Annu. Rev. Phys. Chem.* **2008**, *59*, 713.
(5) Silverman, D. N.; McKenna, R. *Acc. Chem. Res.* **2007**, *40*, 669.
(6) Hoerner, J. K.; Xiao, H.; Dobo, A.; Kaltashov, I. A. *J. Am. Chem. Soc.* **2004**, *126*, 7709.
(7) Marx, D.; Tuckerman, M. E.; Hutter, J.; Parrinello, M. *Nature* **1999**, *397*, 601.
(8) Dayie, K. T.; Wagner, G. *J. Am. Chem. Soc.* **1997**, *119*, 7797.
(9) Slebockatilk, H.; Bennet, A. J.; Hogg, H. J.; Brown, R. S. *J. Am. Chem. Soc.* **1991**, *113*, 1288.
(10) Deakyne, C. A.; Meot-Ner, M.; Cynthia, L. C.; Michael, G. H.; Sean, P. M. *J. Chem. Phys.* **1986**, *84*, 4958.
(11) Meot-Ner, M. *Chem. Rev.* **2005**, *105*, 213.
(12) Wei, S.; Tzeng, W. B.; Castleman, A. W. *J. Phys. Chem. A* **1991**, *95*, 585.
(13) Wei, S.; Tzeng, W. B.; Keesee, R. G.; Castleman, A. W. *J. Am. Chem. Soc.* **1991**, *113*, 1960.
(14) Kebarle, P.; Haynes, R. M.; Collins, J. G. *J. Am. Chem. Soc.* **1967**, *89*, 5753.
(15) Stace, A. J.; Shukla, A. K. *J. Am. Chem. Soc.* **1982**, *104*, 5314.
(16) Stace, A. J.; Moore, C. *J. Am. Chem. Soc.* **1983**, *105*, 1814.
(17) Wu, C. C.; Jiang, J. C.; Boo, D. W.; Lin, S. H.; Lee, Y. T.; Chang, H. C. *J. Chem. Phys.* **2000**, *112*, 176.
(18) Jiang, J. C.; Chaudhuri, C.; Lee, Y. T.; Chang, H. C. *J. Phys. Chem. A* **2002**, *106*, 10937.
(19) Chaudhuri, C.; Jiang, J. C.; Wang, X.; Lee, Y. T.; Chang, H. C. *J. Chem. Phys.* **2000**, *112*, 7279.
(20) Suhara, K.; Fujii, A.; Mizuse, K.; Mikami, N.; Kuo, J. L. *J. Chem. Phys.* **2007**, *126*, 194306.
(21) Meot-Ner, M. *J. Am. Chem. Soc.* **1986**, *108*, 6189.
(22) Lyktey, M. M. Y.; DeLeon, R. L.; Shores, K. S.; Furlani, T. R.; Garvey, J. F. *J. Phys. Chem. A* **2000**, *104*, 5197.
(23) Herron, W. J.; Coolbaugh, M. T.; Vaidyanathan, G.; Peifer, W. R.; Garvey, J. F. *J. Am. Chem. Soc.* **1992**, *114*, 3684.
(24) Wu, C. C.; Chaudhuri, C.; Jiang, J. C.; Lee, Y. T.; Chang, H. C. *J. Phys. Chem. A* **2004**, *108*, 2859.
(25) Karpas, Z.; Eiceman, G. A.; Harden, C. S.; Ewing, R. G.; Smith, P. B. W. *Org. Mass Spectrom.* **1994**, *29*, 159.
(26) Chang, H. C.; Jiang, J. C.; Hahndorf, I.; Lin, S. H.; Lee, Y. T.; Chang, H. C. *J. Am. Chem. Soc.* **1999**, *121*, 4443.
(27) Karpas, Z.; Eiceman, G. A.; Ewing, R. G.; Harden, C. S. *Int. J. Mass Spectrom. Ion Processes* **1994**, *133*, 47.
(28) Hunter, E. P. L.; Lias, S. G. *J. Phys. Chem. Ref. Data* **1998**, *27*, 413.
(29) Fridgen, T. D.; McMahon, T. B.; MacAleese, L.; Lemaire, J.; Maitre, P. *J. Phys. Chem. A* **2004**, *108*, 9008.
(30) Fujii, A.; Enomoto, S.; Miyazaki, M.; Mikami, N. *J. Phys. Chem. A* **2005**, *109*, 138.
(31) Kuo, J. L.; Fujii, A.; Mikami, N. *J. Phys. Chem. A* **2007**, *111*, 9438.
(32) Kuo, J. L.; Klein, M. L. *J. Chem. Phys.* **2005**, *122*, 24516.
(33) Kazimirski, J. K.; Buch, V. *J. Phys. Chem. A* **2003**, *107*, 9762.
(34) Miyazaki, M.; Fujii, A.; Ebata, T.; Mikami, N. *Science* **2004**, *304*, 1134.
(35) Wu, C. C.; Lin, C. K.; Chang, H. C.; Jiang, J. C.; Kuo, J. L.; Klein, M. L. *J. Chem. Phys.* **2005**, *122*, 074315.
(36) Jiang, J. C.; Chang, H. C.; Lee, Y. T.; Lin, S. H. *J. Phys. Chem. A* **1999**, *103*, 3123.
(37) Khan, A. *Chem. Phys. Lett.* **1994**, *217*, 443.
(38) Shin, J. W.; Hammer, N. I.; Diken, E. G.; Johnson, M. A.; Walters, R. S.; Jaeger, T. D.; Duncan, M. A.; Christie, R. A.; Jordan, K. D. *Science* **2004**, *304*, 1137.
(39) Singh, N. J.; Park, M.; Min, S. K.; Suh, S. B.; Kim, K. S. *Angew. Chem., Int. Ed.* **2006**, *45*, 3795.
(40) Chang, H. C.; Jiang, J. C.; Lin, S. H.; Lee, Y. T.; Chang, H. C. *J. Phys. Chem. A* **1999**, *103*, 2941.
(41) Burt, M. B.; Fridgen, T. D. *J. Phys. Chem. A* **2007**, *111*, 10738.
(42) Fridgen, T. D. *J. Phys. Chem. A* **2006**, *110*, 6122.
(43) Fridgen, T. D.; MacAleese, L.; McMahon, T. B.; Lemaire, J.; Maitre, P. *Phys. Chem. Chem. Phys.* **2006**, *8*, 955.

(44) Gardenier, G. H.; Roscioli, J. R.; Johnson, M. A. *J. Phys. Chem. A* **2008**, *112*, 12022.
(45) Roscioli, J. R.; McCunn, L. R.; Johnson, M. A. *Science* **2007**, *316*, 249.
(46) Kuo, J.-L.; Xie, Z.-z.; Bing, D.; Fujii, A.; Hamashima, T.; Suhara, K.-i.; Mikami, N. *J. Phys. Chem. A* **2008**, *112*, 10125.
(47) Jackson, P. *Int. J. Mass Spectrom.* **2004**, *232*, 67.
(48) Frisch, M. J. T. et al. *Gaussian 03*; Gaussian, Inc.: Wallingford, CT, 2004.
(49) Wang, Y. S.; Chang, H. C.; Jiang, J. C.; Lin, S. H.; Lee, Y. T.; Chang, H. C. *J. Am. Chem. Soc.* **1998**, *120*, 8777.

JP900066U